Intermittent Theta Burst Stimulation Drives Bi-Directional Changes in Excitability in Prefrontal Cortex

Morteza Salimi [1,2#], Milad Nazari [3-5#], Jonathan Mishler[1,2], Jyoti Mishra[2], Dhakshin S Ramanathan [1,2*]

1. Mental Health Service, VA San Diego Healthcare Syst., La Jolla, CA, 92161
2. Dept. of Psychiatry, UC San Diego, La Jolla, CA, 92093
3. Department of Molecular Biology and Genetics, Aarhus University, Aarhus, Denmark
4. DANDRITE, The Danish Research Institute of Translational Neuroscience, Aarhus, Denmark
5. Center for Protein in Memory-PROMEMO, Danish National Research Foundation

# These authors contributed equally

*Corresponding authors
Dhakshin Ramanathan
Email:dramanathan@health.ucsd.edu

Abstract

Theta burst stimulation (TBS), an FDA-cleared treatment for depression, is hypothesized to modulate excitability in the prefrontal cortex, though this has not definitively been shown in vivo. We performed calcium imaging on glutamatergic neurons in awake rodents to understand the effects of theta burst stimulation at a cellular level. Our findings provide the first direct evidence that TBS bidirectionally modulates glutamatergic activity when delivered in vivo and directly links calcium activity changes during stimulation with post-stimulation plasticity.

Main

Repetitive transcranial magnetic stimulation (rTMS) has been used in experimental research studies for over 4 decades as a non-invasive tool to temporarily modulate excitability in the human brain. While various stimulation protocols are used, a common one is Theta Burst Stimulation (TBS)[1,2], a protocol recently FDA-cleared to treat depression[3]. TBS involves a burst of a 3-4 pulses delivered at 50-100Hz, with each burst delivered every 200ms, e.g. at a 5Hz theta rhythm, for 2 seconds[4]. It was first used in the 1980s as a physiologically plausible method for inducing long-term-potentiation in hippocampal slices[2,4]. Experimental studies in humans have suggested that repeated trains (typically 20) of TBS may affect motor evoked potentials, a noninvasive marker of cortical excitability[1,5–7]. Surprisingly, this research showed that when repeated TBS trains are separated by a short inter-train interval they result in a net decrease in motor evoked potentials (i.e. diminished excitability) whereas when the inter-trial interval between trains was extended to 10 seconds, there was a net increase in motor evoked potentials/excitability[1,5,6]. To date, this core bi-directionality of TBS in modulating markers of excitability remains unexplained and there is little direct data that intracortical excitability of single cells is even modulated by TBS delivered in vivo[8].

In this paper, we aim to address these gaps in knowledge. We applied imaging cellular activity (using an implanted 1-photon miniaturized microscope[9]) immediately prior to, during and for 40 minutes after the delivery of TBS (**Figure 1A-D)** . All animals received 20 trains of a 2s TBS with varying inter-train intervals from 4 up to 40s[1]. The inter trial interval (ITI) here is defined from the start of the trains thus an ITI of 4s consists of a 2s pause between the 2s trains.

We first found that while one set of neurons showed the expected increase in calcium levels during stimulation ('excited' cells), other neurons surprisingly showed a reduction in calcium levels during TBS ('inhibited' cells) (**Fig 1E).** Across the various TBS paradigms tested, 32.8% of cells showed calcium suppression (inhibition) while 39.6% of cells showed an increase in

calcium (excitation) during stimulation (**Fig 1F-G)**. No significant differences were observed in the proportion of cells that were excited vs. inhibited between the various ITI protocols. We next quantified the mean change in calcium levels during stimulation separately for excited and inhibited cells during TBS (**Fig 1H-P)**. We found a stepwise decrease in both calcium excitation (**Fig 1N;** $F_{(4,2717)}$=150.8, p<0.0001) and inhibition (**Fig 1O;** $F_{(4,2307)}$=101.6, p<0.0001) with increasing ITI. Post-hoc tests showed these effects reached a plateau at 20s ITI and 40s ITI respectively (Table S1). The net effect of stimulation (combining excited and inhibited cells and averaging across the entire population) looked generally similar to the excited alone cells (**Fig P,** $F_{(4,5026)}$=82.44, p<0.0001**)**. This suggests that coarser methods of brain imaging (for example, fiber photometry, EEG or fMRI) would miss the suppressive effects of stimulation we observed here at the level of single cells.
We next examined the relationship between calcium excitation/inhibition during TBS and long-term changes in calcium levels post-TBS. The population of cells that were excited during TBS showed a long-term increase in calcium activity in the 40-minute period post stimulation for ITIs above 4s **(Fig 2A)**. In fact, in excited cells, there was a stepwise increase in calcium levels post TBS with increasing ITI, the exact opposite effect we observed in calcium levels during TBS (ANOVA: main effect of ITI, $F_{(4,24426)}$=174.8, p<0.0001; time: $F_{(8,24426)}$=41.63, p<0.0001; interaction effect: $F_{(32,24426)}$=4.85, p<0.0001). Post-hoc analyses focused on the main effect of ITI demonstrated a significant increase in the post-TBS modulation of excited cells up to 20s. We performed a similar analysis for the cells that were inhibited during TBS (**Fig 2C)** and found a similar stepwise increase in post TBS inhibition with increasing ITI (ANOVA: main effect of ITI $F_{(4,20763)}$=47.88, p<0.0001; time-effect: $F_{(8,20763)}$=58.29, p<0.0001 and interaction effect: $F_{(32,20763)}$=1.26, p=0.14). Post-hoc analyses again demonstrated a significant increase in post-TBS suppression of calcium activity up to 20s ITI. (Table S2) Thus, we found that with increased ITI there was a stronger long-term bi-directional modulation of calcium activity, with effects peaking around 20s. Given these bi-directional effects, we analyzed the “net” change in calcium activity by averaging across all neurons from these two groups to get a marker of overall changes in excitability. Using this approach (**Fig 2D),** we found a main effect of ITI ($F_{(4,45234)}$=21.22, p<0.0001). Post-hoc tests showed that the 20s ITI on balance showed a greater increase in net calcium activity compared to all other ITIs other than the 40s ITI; while the 4s ITI showed a greater net inhibition in calcium activity compared to all other manipulations in this later time-period (Table S2). The 20s and 40s ITI both showed an overall net increase in calcium compared to baseline (p<0.001 and p<0.01 respectively, one-sample t-test) and the 4s ITI showed an overall net inhibition in calcium compared to baseline (one-sample t-test, p<0.001). Thus, roughly in-line with data from humans, we find that TBS with short ITIs show a net inhibition of glutamatergic calcium activity while longer ITIs (especially 20-40s), showed an overall net increase in glutamatergic calcium activity in the 40min period post stimulation. Interestingly, our data suggests that a slightly longer ITIs (20s) might work better than the current FDA-cleared protocol, which uses a 10s ITI. Moreover, these results suggesting 10sTBS shows a balanced effect on cells may help explain some of the heterogeneity in long-term effects of TBS observed in humans[10].

Results shown in Fig 2B-C above suggest that for both excited and inhibited cells, extended ITIs were overall more effective at driving related changes in calcium levels post-TBS. To further understand this, we performed a correlation between calcium change during TBS and long-term changes in calcium activity post TBS for different ITIs (**Fig 2E)**. The 4s ITI showed a small but significant relationship between these two factors (r = 0.15, p<0.0001). The 10s ITI showed a stronger relationship (r= 0.32 , p<0.0001) and the 20s ITI showed the strongest relationship between the two (r=0.63, p<0.0001), with correlation values significantly different from each other (**Fig 2F**)**.** The change in correlation with increased ITI was at least partially linked to the fact that, at ITIs > 4s, more TBS-excited cells remained elevated post-TBS (**Fig 2G)**.

Quantification showed this effect was significantly different for the 4s ITI compared to longer ITIs (**Fig 2G**, Mann Whitney test, $\chi^2 = 6.48$, $p=0.01$**)**.
Our main findings, above, could be explained by the fact that TBS activates both excitatory and inhibitory inputs onto cells being imaged. Neurons that are suppressed during stimulation have on balance more stimulation-evoked inhibition compared to cells that were excited and thus, post TBS, when both inhibitory and excitatory inputs to cells are strengthened, these cells end up showing long-term inhibition of activity. In this model, cells that are activated during TBS but then show a post TBS suppression would also have greater inhibitory tone during/after TBS compared to cells that show a post TBS excitation. To test this, we examined the TBS-induced stimulation waveform in more detail (**Fig 3A-C**). We found (particularly at ITIs above 4s), that cells that show a long-term excitation post TBS have a release of inhibition starting around 5 seconds post TBS compared to cells that show long-term inhibition post TBS (this was true for both TBS-excited and TBS-inhibited cells). Notably, this effect/separation typically started around 5s post TBS and was minimally observable at the 4s ITI, suggesting that prior to that 5s window, there is still significant amounts of inhibitory inputs on all cells.
This data further suggests that TBS performed with short ITI stimulation protocols (particularly < 5 seconds) occur during greater levels of inhibitory tone, which is known to limit LTP-like effects and bias cells towards LTD [11,12]. As a final analysis to see if there was greater GABAergic tone on neurons at the 4s ITI, we compared the stimulation/decay slopes during/after TBS for excited and inhibited cells. For excited cells, we focused on the decay slope in the 2s immediately after TBS (**Fig 3D** $F_{(4, 76)}=20.53$, $p<0.0001$**)**, using the slope of decay as a proxy for evoked inhibitory tone. We found a significant effect of ITI, with short ITI having the greatest negative slope (i.e. highest level of inhibitory tone). The inhibitory neurons showed an even more interesting pattern calcium was suppressed during the TBS, but only for the 4s ITI; at extended ITIs, the inhibition occurred post TBS in the inter-trial interval ($F_{(3.3\ 64.2)}=115.1$, $p<0.0001$; **Fig 3E**). Thus, our data from two distinct analyses suggest that the inhibitory tone during and immediately after 4s ITI TBS may account for the bidirectional effects of TBS when comparing short versus long ITIs. In this study we provide the first direct mechanistic evidence connecting calcium influx during repetitive TBS trains with long-term changes in excitability in vivo, showing that TBS exerts bi-directional modulations of activity likely driven by GABAergic activity. Moreover, we found a novel 20s ITI protocol that could be more effective than standard iTBS in driving excitability in the brain.

Figure 1. Protocol of study and calcium level during TBS. (A) The schematic shows animals implanted with a TDT adaptor for electrical stimulation and an Inscopix miniscope lens for single-cell calcium imaging. (B) A screenshot from Inscopix Data Processing shows excited and inhibited cells within the implanted lens field of view. (C) Histological verification of virus expression is shown in green, indicating the expression region within the medial prefrontal cortex. (D) Theta burst stimulation (TBS) was delivered with 3 pulses at 50 Hz between pulses and 5 Hz between trains, with inter-train intervals varying between recording sessions. Rats received 20 trains, each comprising 10 bursts per train with variable ITIs, followed by 5 minutes of baseline recording. Each bar represents a stimulation train. Recordings continued for 40 minutes post-TBS. (E) Cell responses to stimulation trains were classified as excited or inhibited by comparing their average activity in 4-second time bins during stimulation to baseline activity. (F) proportion of cell categories for different ITIs. Extending decreases excited cells and increases inhibited cells during TBS. (G) Proportional changes across

ITIs (Chi-square statistic, X^2=3.87, p=.42). **(H-J)** Z-score for whole cell activity during entire recording session. **(K-M)** Z-score for cell population responses to TBS periods. The upper panels indicate activity for the entire cell population (black), lower panels show activity for excited (red) and inhibited (blue) populations. Cells were sorted based on significant activity changes compared to baseline (p < 0.01). Average Z-score activity during and post-TBS for varying stimulation periods across all recorded cells (n=1384 for ITI 4; n=1262 for ITI 10; n=1119 for ITI 20). **(N-P)** Average Z-score of cell response to different stimulation ITI protocols (color-coded from red to blue, 4 to 60 seconds ITIs) across the entire recording session. The grey shaded area corresponds to values in the bottom panels which indicates the average Z-score response during the TBS period among different cell populations. Extending ITI leads to a decrease in the response of excited cells, reduced response in the inhibited cell population, and an overall decrease when combining excited and inhibited cells. No significant changes were found for comparing ITIs of 20, 40, and 60s. Data were analyzed using repeated measures ANOVA followed by Sidak's correction for multiple comparisons. Values are mean ± SEM. ***p < 0.001, ****p < 0.0001.

Figure 2. Extended theta burst stimulation (eTBS) enhances long-term plasticity: **(A)** Post TBS Z-score for single-cell activity, excited cells (left) and inhibited cells (right). shaded area indicates TBS period. The Z-score activity of cells was calculated by normalizing their activity throughout the entire session to their baseline activity recorded during the 5 minutes prior to the onset of TBS. Cells were classified as excited, inhibited or non-responsive during TBS by comparing their average activity in 4 second time bins during these periods to the binned activity during the baseline period using the Wilcoxon rank-sum test in MATLAB ($p< 0.01$). **(B-D)** Average activity over time in sorted populations in excited, inhibited and net (excited/inhibited) respectively (left), with every 5 minutes binned data. The right panel shows the average activity across 40 minutes post-TBS. Extending the inter-trial interval (ITI) leads to a stronger response in both excited and inhibited cells. Combining the data for populations (excited/inhibited) shows that extending TBS to 20 seconds significantly increases activity for 40 minutes post TBS. One sample t-test comparison with zero indicates a significant reduction in ITI4 and significant increase in ITI 20 and 40. Stim conditions are color coded (red to blue, 4 to 60 ITIs). Data were analyzed using ANOVA followed by Sidak's correction for multiple comparisons. Values are mean ± SEM. *p < 0.05, **p < 0.01, ***p < 0.001, ****p < 0.0001; one-sample t-test compared with zero, ##p < 0.01; ###p < 0.001. **(E)** Correlation between during and post TBS Z-score activity among the net population (Excited/inhibited cells). **(F)** Extending ITI significantly increases the correlation coefficient. Data were analyzed using linear regression with X=during TBS and Y=post-TBS. Pearson correlation coefficient, **p < 0.01, ***p < 0.001 and ****p < 0.0001.
(G) Consistency of cell activity during vs post TBS in the response to extending ITIs. Excited and inhibited cells marked as red and blue respectively. Size of arrows and shapes are regulated based on cell numbers (digits in the shapes). Extending ITI increases excited cells consistency by decreasing transiting excited cells during TBS to inhibited cells after TBS. The McNemar test revealed a statistically significant difference in proportions cells categories during versus post TBS for ITI4 (χ^2 = 6.48, p=0.01). No

significant difference reported for ITI 10 to 60. (ITI 10, $\chi^2 = 1.4$, $p=0.2$; ITI 20, $\chi^2 = 0.43$, $p=0.51$; ITI 40, $\chi^2 = 0.74$, $p=0.1$; ITI 60, $\chi^2 = 1.0$, $p=0.3$;).

Figure 3. Extended theta burst stimulation (eTBS) improves inter trial interval short term plasticity. (A) The top panel illustrates the timing of the stimulation, showing 20 trials with 10 bursts each. The middle panel displays the overall cellular response to TBS trials, with red dashed lines marking the epochs of trials and the orange shaded area indicating the burst period. The bottom panel shows the average response across 20 trials. **(B)** Illustrates the persistence of excited cells during TBS that remain excited postTBS versus excited cells that become inhibited post-TBS. Excited cells within ITI 4 shows a decrease in activity after the stimulation period and return to resting activity during ITI period. At an ITI of 4 seconds, there were no significant differences between cells that were excited both during and after TBS and those that were excited during but inhibited after TBS. However, extending the ITI led to a significant distinction between these groups. The separation time is approximately 3.5 seconds (3.1 seconds for ITI 10 and 4.6 seconds for ITI 20). **(C)** The significant separation time for inhibited neurons during ITI 4 TBS is limited to a narrow time window of 3.2 seconds up to end of the ITI, showing significant changes between inhibited-during excited-post and inhibited-during inhibited-post TBS. For extended TBS, this separation begins around 4.19 seconds for ITI 10 and 2.8 seconds for ITI 20 which were sustained to the end of the ITI. The orange bar illustrates the stimulation period, and lines with shaded areas indicate mean ± SEM. Data were analyzed using paired t-tests with corrected p-values for multiple time point comparisons, with the green shaded area indicating $p < 0.05$. **(D)** Trial-by-trial average responses of the population of excited (left) and inhibited (right) cells to varying ITIs. The orange shaded area marks the burst stimulation period, consistent across different ITIs (n=1384 for ITI 4; n=1262 for ITI 10; n=1119 for ITI 20). Extending ITI indicates a longer decay time for excited cells to return to baseline. **(E)** During TBS with a ITI 4, calcium levels were suppressed while at extended ITIs, this suppression shifted to occur post-TBS during the inter-trial interval. Data were analyzed using repeated measures ANOVA followed by Sidak's correction for multiple comparisons. Values are presented as mean ± SEM (**$p < 0.01$, ***$p < 0.001$, ****$p < 0.0001$).

Materials and methods

Subjects

The study utilized five female Long Evans rats, sourced from Charles River Laboratories. Upon arrival, the rats were approximately one month old, weighing around 150 grams. They were acclimated to the laboratory environment for two weeks prior to surgery. During this period, the rats were housed in pairs in standard plastic tubs (10 × 10.75 × 19.5 in, Allentown, NJ, USA). Following the surgical procedure, the rats were single housed to facilitate post-operative care and recovery. The housing environment was maintained on a 12-hour light/dark cycle, with lights on at 6 a.m., and all experimental testing was conducted during the light cycle. Throughout the study, the rats had ad libitum access to food and water, ensuring consistent nutrition and hydration. At the start of the recording phase, the rats were aged between 3 to 5 months and weighed between 300 to 600 grams.

Electrolens Fabrication

To enable the delivery of theta burst stimulation (TBS), we constructed an electrolens assembly by attaching four 50 µm tungsten wires (California Fine Wire) alongside the lens using epoxy. These wires were spaced 100 µm apart, starting from beneath the lens edge. The electrodes that demonstrated the most effective stimulation impact on calcium imaging were chosen for

TBS delivery. For the ground connection, a 75 µm annealed stainless-steel wire, approximately 10 cm in length, was used (A-M Systems, Loop Sequim, WA, USA). The ground wire was soldered to a self-tapping stainless steel bone screw measuring 5.20 mm in length and 1.15 mm in width (Fine Science Tools).

Surgical Procedure

Stereotaxic surgery was performed using sterile techniques to implant both recording and stimulation probes. All surgical instruments were autoclaved prior to the procedure. Rats were anesthetized in an induction chamber using 5% isoflurane in 96% room air, delivered by a low-flow anesthetic machine (Kent Scientific, Torrington, CT, USA). Once deeply anesthetized, the rats were placed in a stereotaxic frame, and anesthesia was maintained at 1.9–2.5% isoflurane through a nose cone for the remainder of the surgery. A body temperature-controlled heating mat (VWR, Radnor, PA, USA) maintained the body temperature at 37 °C. To reduce surgical risks, rats received a single dose of Atropine (0.05 mg/kg) to minimize respiratory secretions, a single dose of Dexamethasone (0.5 mg/kg) to reduce inflammation, and 1 mL of 0.9% sodium chloride solution for hydration. The surgical site was sterilized with 70% ethanol and iodine solution. Lidocaine (0.2 cc max) was administered as a local anesthetic at the incision site. An incision was made to expose the skull, and the skin was held back using four skin clamps. Cranial holes for anchor and ground screws were drilled at the periphery of the exposed skull using a 0.7 mm (Stoelting). A ground screw and wire were secured posterior to the lambda point on the skull, while 3-5 anchor screws were inserted around the periphery of the skull. The screws were fixed in place using C&B Metabond (Parkell, Inc., Edgewood, NY, USA) applied to the dried skull surface. Coordinates relative to bregma and lambda were used to identify the target location in the medial prefrontal cortex (mPFC) AP=+4.2 mm , ML=0.7mm. A 1.2 mm diameter hole was drilled using a trephine drill bit. A ready-to-use viral vector targeting pyramidal neurons was injected into the mPFC using a 33-gauge Hamilton syringe and a WPI micro infusion pump at a rate of 100 nL/min, with the needle reaching a depth of DV = 2.8 mm. After injection, the needle remained in place for 10 minutes before being withdrawn to ensure diffusion. A guide cannula was then lowered to a depth of DV = 2.1 mm at a rate of 1 mm/sec and slowly withdrawn. A 1 mm diameter, 9 mm length integrated ProView lens was implanted at a depth of DV = 2.4 mm at a rate of 0.5 mm/sec. The gap between the lens and brain surface was sealed using Kwik-Sil (WPI) to prevent damage and maintain stability. The lens was then secured with black dental cement. The wires were connected to a TDT ZCA-EIB32 ZIF-Clip® Headstage to Electrode Interface Board. Post-surgery, the animals were removed from the stereotaxic frame and allowed to recover on a heating pad. Recovery was monitored, and analgesics were administered as needed to ensure animal welfare.

This study adhered to the guidelines outlined in the Guide for the Care and Use of Laboratory Animals of the National Institutes of Health. The research protocol received approval from the Institutional Animal Care and Use Committee (IACUC) at the San Diego VA Medical Center (Protocol Number A12-021).

Single photon Ca^{2+} Imaging.

Calcium imaging was performed using a miniature microscope (nVoke 2.0, Inscopix) equipped with a 1 mm diameter lens, enabling the visualization of neuronal activity in freely moving animal. Prior to the experiment, the optimal LED power, gain settings, and lens focus were meticulously adjusted to ensure the clearest possible representation of neurons within the field of view. Data acquisition was conducted at a frame rate of 20 Hz, which was later down-sampled both spatially and temporally by a factor of 3 to optimize data quality and processing efficiency. Images were bandpass filtered (0.005-0.5 Hz) and corrected for any potential motion artifacts using the Inscopix Data Processing Software (IDPS). The constrained nonnegative matrix factorization for microendoscopic data (CNMF-E) algorithm was utilized to accurately

detect and extract cellular activity. A subsequent manual verification process was conducted to exclude any non-cellular objects, ensuring that only genuine neuronal signals were analyzed.

Data Processing

Matlab v2023a was used for data analysis. Cell classification was based on the Z-score normalization of cellular activity throughout the entire recording session, using baseline activity recorded during the 5 minutes preceding the onset of TBS as the reference. Cells were classified as excited, inhibited, or non-responsive based on their average activity in 4 sec time bins during TBS and post-TBS periods, compared to the baseline period. This classification was conducted using the Wilcoxon rank-sum test in MATLAB, with a significance threshold set at $p<0.01$.

To calculate the raising and decay slopes, we used the period from 5% to 95% of the TBS and the 2 seconds immediately following the TBS, respectively. We then reported the slope of the fitted line using the *polyfit* function in MATLAB.

To evaluate the relationship between average neuronal activity during TBS and post-TBS periods, a linear regression model was implemented in MATLAB. This model facilitated the assessment of the correlation between Z-score values in these periods. The estimated regression coefficients and their corresponding p-values were reported, providing insights into the stability and consistency of neural responses across different stimulation intervals.

Theta burst Stimulation protocol.

TBS Protocol

Theta Burst Stimulation (TBS) was administered using a precise and controlled protocol designed to modulate neuronal activity effectively. The stimulation was delivered through a Tucker-Davis Technologies (TDT) IZ2 stimulation device, utilizing ZIF-Clip® ZC Analog Headstages to ensure accurate and reliable signal transmission. The TBS protocol consisted of bursts of stimulation with the following parameters: each burst comprised 3 pulses, delivered as a square wave with a cathodal leading configuration. The amplitude of each pulse was set to 100 microamps, providing a consistent and robust stimulation across sessions. Each train of stimulation included 10 bursts, with a total of 20 trains administered per session (Fig S1).

To facilitate the delivery of these stimulation parameters, the setup included carefully positioned tungsten electrodes attached beside the imaging lens, allowing for precise targeting of the medial prefrontal cortex. The TDT device was configured to synchronize the timing and intensity of the pulses accurately, ensuring reproducibility and control over the stimulation conditions. This setup allowed for the exploration of how different temporal patterns of stimulation influence neuronal dynamics and plasticity.

Histological verifications

To verify viral expression in the medial prefrontal cortex, brain tissue was processed and analyzed. Following behavioral experiments, rats were deeply anesthetized and transcranial perfused with 0.9% saline followed by 4% paraformaldehyde (PFA) in phosphate-buffered saline (PBS). Brains were extracted and post-fixed in 4% PFA overnight at 4°C, then cryoprotected in 30% sucrose in PBS until they sank. Coronal sections of 40 µm thickness were prepared using a cryostat (Leica CM1950, Leica Biosystems) and collected on gelatin-coated glass slides. Sections were air-dried, rehydrated in PBS, and counterstained with DAPI (4′,6-diamidino-2-phenylindole) to visualize cell nuclei. Coverslips were applied using an antifade mounting medium (Fluoromount-G). Confocal microscopy was used to visualize the expression of the viral vector. Imaging was performed using a confocal microscope (Zeiss LSM 880, Zeiss Microscopy) equipped with lasers for blue (405 nm) and green (488 nm) fluorescence. The presence of green fluorescent protein (GFP) signal, indicating successful viral expression, was detected in the prefrontal cortex. Fluorescence images were captured and analyzed using the

accompanying software (Zeiss ZEN). To confirm the anatomical accuracy of viral expression, fluorescence images were compared to the Paxinos and Watson rat brain atlas. Images were matched to the closest anterior-posterior coordinates, ensuring that the expression was localized to the medial prefrontal cortex. This verification confirmed that the viral delivery targeted the intended brain region, supporting the reliability of the subsequent analyses. By integrating these histological techniques, we ensured precise confirmation of viral expression within the targeted neural circuits, facilitating the interpretation of the behavioral and physiological effects observed.

Statistical Analysis

Statistical analyses were conducted to evaluate the effects of extended theta burst stimulation (eTBS) on cellular activity across different inter-train intervals (ITIs). A mixed-effects model two-way ANOVA was used to compare post-TBS effects across time bins among different ITIs, allowing us to assess interactions between time and treatment. To analyze differences during the TBS window, a one-way ANOVA was employed to compare the activity between ITIs. Post-hoc comparisons following ANOVA were corrected using Sidak's correction for multiple comparisons. Data are presented as mean ± SEM. To investigate the relationship between during-TBS and post-TBS activity, linear regression analysis was performed with post-TBS activity as the dependent variable (Y) and during-TBS activity as the independent variable (X). The results were reported with 95% confidence intervals, the R-squared value to indicate the goodness of fit, and Pearson's correlation coefficient to assess the strength and direction of the relationship. The McNemar test was applied to evaluate the effects of different ITIs on the proportion of cell categories during versus post-TBS. This test compared the proportion of excited cells (positive observations) to inhibited cells (negative observations) before and after TBS. Statistical significance was considered at $p < 0.05$ for all tests. All statistical analyses were performed using IBM SPSS Statistics Version 29. Data visualization and plotting were conducted using GraphPad Prism.

Funding sources: This work was supported by the Burroughs Wellcome fund (1015644 to DR), the National Institutes for Health (1R01MH123650 to DR), start-up funds from the UCSD Department of Psychiatry (to DR), and the VA Office of Research and Development (Career Development Award to DR. Hope for Depression Research Foundation award to JM.

References

1. Huang, Y.-Z., Edwards, M. J., Rounis, E., Bhatia, K. P. & Rothwell, J. C. Theta Burst Stimulation of the Human Motor Cortex. *Neuron* **45**, 201–206 (2005).
2. Larson, J. & Munkácsy, E. Theta-burst LTP. *Brain Research* **1621**, 38–50 (2015).
3. Blumberger, D. M. *et al.* Effectiveness of theta burst versus high-frequency repetitive transcranial magnetic stimulation in patients with depression (THREE-D): a randomised non-inferiority trial. *The Lancet* **391**, 1683–1692 (2018).
4. Larson, J., Wong, D. & Lynch, G. Patterned stimulation at the theta frequency is optimal for the induction of hippocampal long-term potentiation. *Brain Research* **368**, 347–350 (1986).
5. Desforges, M. *et al.* Dose-response of intermittent theta burst stimulation of the prefrontal cortex: A TMS-EEG study. *Clinical Neurophysiology* **136**, 158–172 (2022).
6. Chung, S. W., Hill, A. T., Rogasch, N. C., Hoy, K. E. & Fitzgerald, P. B. Use of theta-burst stimulation in changing excitability of motor cortex: A systematic review and meta-analysis. *Neuroscience & Biobehavioral Reviews* **63**, 43–64 (2016).
7. Chung, S. W. *et al.* Demonstration of short-term plasticity in the dorsolateral prefrontal cortex with theta burst stimulation: A TMS-EEG study. *Clinical Neurophysiology* **128**, 1117–1126 (2017).

8. Jannati, A., Oberman, L. M., Rotenberg, A. & Pascual-Leone, A. Assessing the mechanisms of brain plasticity by transcranial magnetic stimulation. *Neuropsychopharmacol.* **48**, 191–208 (2023).
9. Stamatakis, A. M. *et al.* Miniature microscopes for manipulating and recording in vivo brain activity. *Microscopy* **70**, 399–414 (2021).
10. Corp, D. T. *et al.* Large-scale analysis of interindividual variability in theta-burst stimulation data: Results from the 'Big TMS Data Collaboration'. *Brain Stimulation* **13**, 1476–1488 (2020).
11. Kotak, V. C., Mirallave, A., Mowery, T. M. & Sanes, D. H. GABAergic inhibition gates excitatory LTP in perirhinal cortex. *Hippocampus* **27**, 1217–1223 (2017).
12. Steele, P. M. & Mauk, M. D. Inhibitory Control of LTP and LTD: Stability of Synapse Strength. *Journal of Neurophysiology* **81**, 1559–1566 (1999).

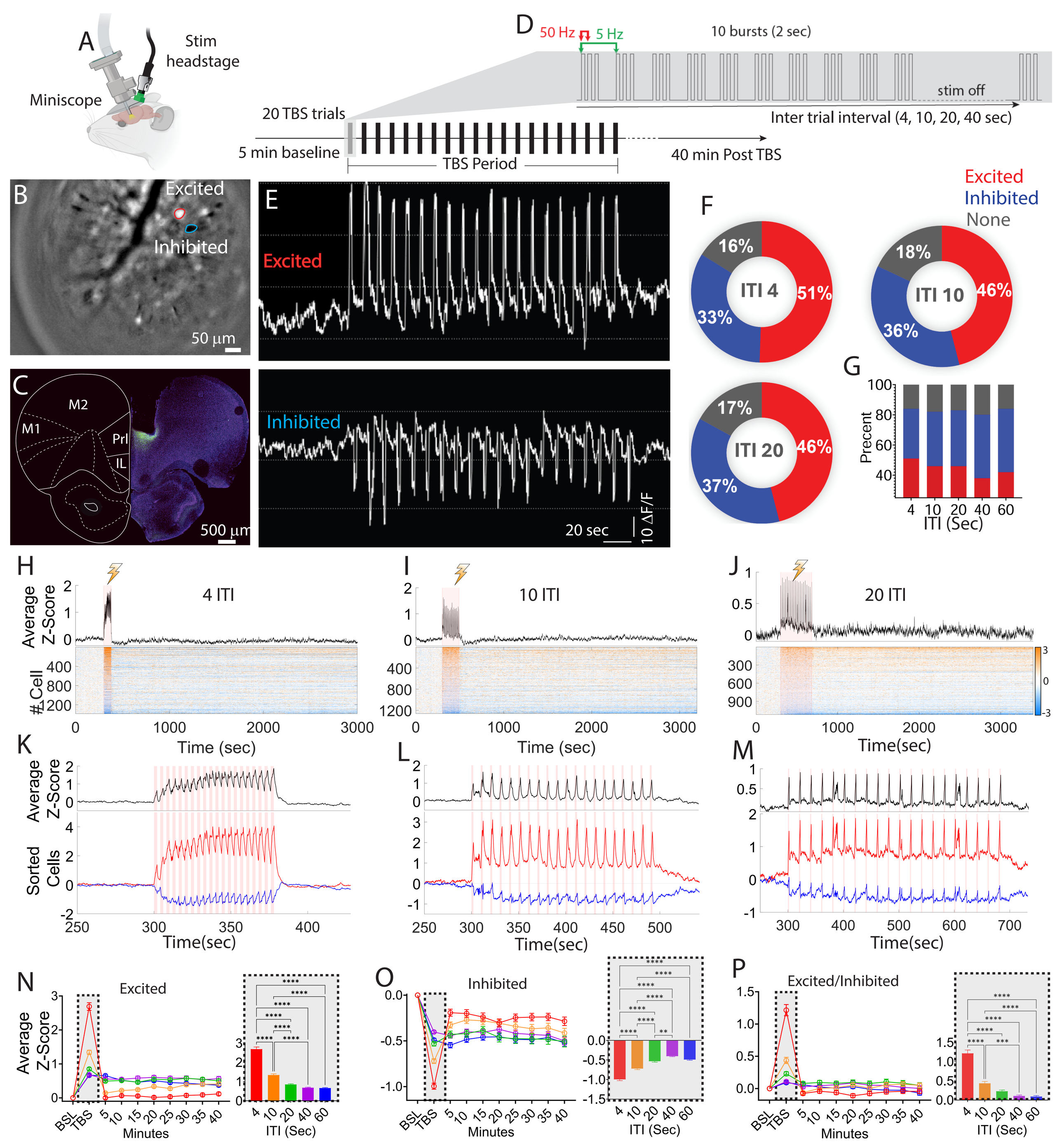
A
Stim headstage
Miniscope
D
50 Hz
5 Hz
10 bursts (2 sec)
stim off
Inter trial interval (4, 10, 20, 40 sec)
20 TBS trials
5 min baseline
TBS Period
40 min Post TBS
B
Excited
Inhibited
50 µm
E
Excited
Inhibited
10 ΔF/F
20 sec
C
M2
M1
PrI
IL
500 µm
F
Excited
Inhibited
None
ITI 4
16%
51%
33%
ITI 10
18%
46%
36%
ITI 20
17%
46%
37%
G
Precent
ITI (Sec)
H
4 ITI
Average Z-Score
#Cell
I
10 ITI
J
20 ITI
K
Time (sec)
Sorted Cells
L
M
Time(sec)
N
Excited
Minutes
ITI (Sec)
O
Inhibited
P
Excited/Inhibited

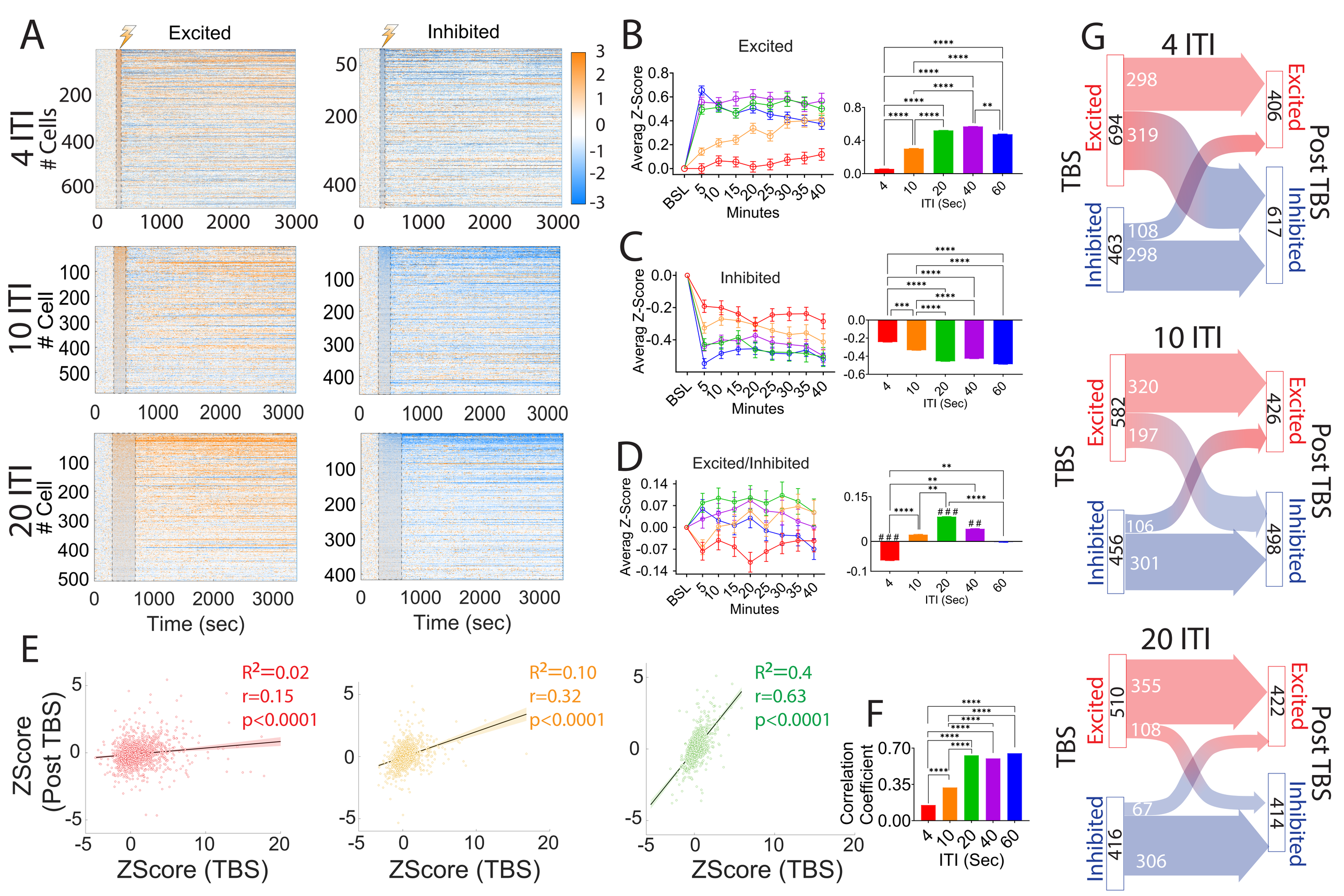
A
Excited
Inhibited
4 ITI
Cells
10 ITI
Cell
20 ITI
Cell
Time (sec)
B
Excited
Averag Z-Score
Minutes
ITI (Sec)
C
Inhibited
D
Excited/Inhibited
E
ZScore (Post TBS)
ZScore (TBS)
R²=0.02
r=0.15
p<0.0001
R²=0.10
r=0.32
p<0.0001
R²=0.4
r=0.63
p<0.0001
F
Correlation Coefficient
G
4 ITI
10 ITI
20 ITI
TBS
Post TBS
Excited
Inhibited
298
319
108
298
694
463
406
617
320
197
106
301
582
456
426
498
355
108
67
306
510
416
422
414

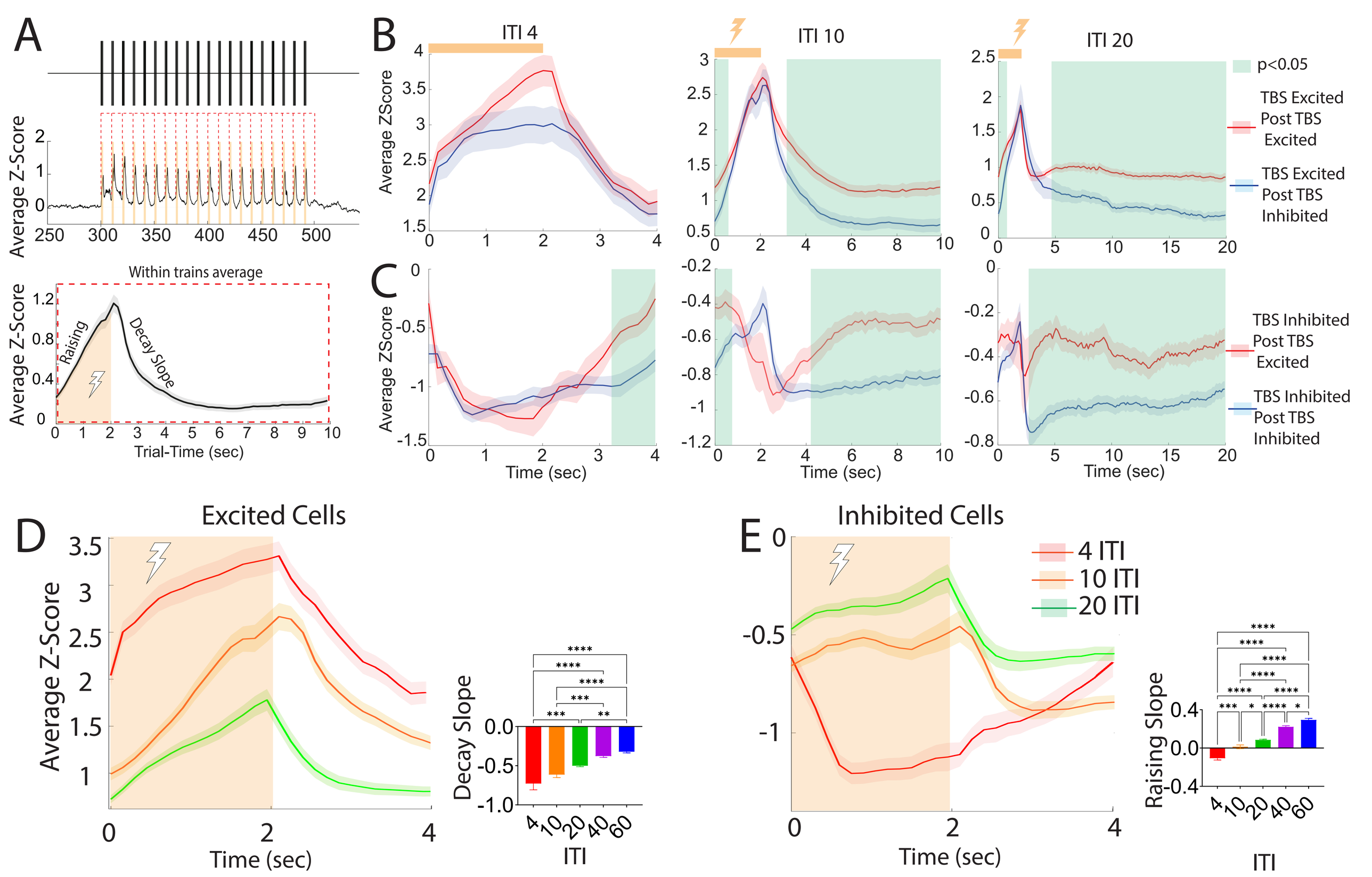
A
Average Z-Score
Within trains average
Raising
Decay Slope
Trial-Time (sec)
B
ITI 4
ITI 10
ITI 20
Average ZScore
p<0.05
TBS Excited Post TBS Excited
TBS Excited Post TBS Inhibited
C
TBS Inhibited Post TBS Excited
TBS Inhibited Post TBS Inhibited
Time (sec)
D
Excited Cells
Average Z-Score
Time (sec)
Decay Slope
ITI
E
Inhibited Cells
4 ITI
10 ITI
20 ITI
Time (sec)
Raising Slope
ITI